3D structure of the C3bB complex provides insights into the activation and regulation of the complement alternative pathway convertase

Eva Torreira[1,*], Agustín Tortajada[1,2,*], Tamara Montes[1,2,*], Santiago Rodríguez de Córdoba[1,2,*] and Oscar Llorca[1,*]

1) Centro de Investigaciones Biológicas, Consejo Superior de Investigaciones Científicas; and 2) Centro de Investigación Biomédica en Enfermedades Raras and Instituto Reina Sofía de Investigaciones Nefrológicas, Ramiro de Maeztu 9, 28040 Madrid, Spain

* All authors contributed equally to this work.

Corresponding authors: Dr. Oscar Llorca
ollorca@cib.csic.es
+34 91 7373112 x4446 (tel)
+34 91 5360432 (fax)

Dr. Santiago Rodríguez de Córdoba**
srdecordoba@cib.csic.es
+34 91 7373112 x4432 (tel)
+34 91 5360432 (fax)

**to whom editorial and production office should communicate

Keywords: C3b, Factor B, C3-convertase, complement, electron microscopy

Running title: Structure of the human C3bB(Ni^{2+}) pro-convertase

Manuscript information: 6 pages, 4 figures, 1 SI text file and 5 supporting figures

Abstract

Generation of the alternative pathway (AP) C3-convertase, the central amplification enzyme of the complement cascade, initiates by the binding of factor B (fB) to C3b to form the pro-convertase, C3bB. C3bB is subsequently cleaved by factor D (fD) at a single site in fB, producing Ba and Bb fragments. Ba dissociates from the complex, whilst Bb remains bound to C3b forming the active AP convertase, C3bBb. Using single-particle electron microscopy we have determined the 3D structures of the C3bB and the C3bBb complexes at ~27Å resolution. The C3bB structure shows that fB undergoes a dramatic conformational change upon binding to C3b. However, the C3b-bound fB structure was easily interpreted after independently fitting the atomic structures of the isolated Bb and Ba fragments. Interestingly, the divalent cation-binding site in the von Willebrand type A domain in Bb faces the C345C domain of C3b whereas the serine-protease domain of Bb points outwards. The structure also shows that the Ba fragment interacts with C3b separately from Bb at the level of the α'NT and CUB domains. Within this conformation the long and flexible linker between Bb and Ba is likely exposed and accessible for cleavage by fD to form the active convertase, C3bBb. The architecture of the C3bB and C3bBb complexes reveals that C3b could promote cleavage and activation of fB by actively displacing the Ba domain from the vWA domain in free fB. These structures provide a structural basis to understand fundamental aspects of the activation and regulation of the AP C3-convertase.

\body

Introduction

Complement is a major component of innate immunity with crucial roles in microbial killing, apoptotic cell clearance and immune complex handling. Complement activation can be initiated by three different pathways: the classical pathway (CP), the alternative pathway (AP), or the lectin pathway (LP). Common to each initiation pathway is the formation of unstable bimolecular complexes, named C3-convertases (AP, C3bBb; CP/LP, C4b2a), which cleave C3 to generate C3b. The AP C3-convertase, C3bBb, is crucial within the complement cascade as it provides exponential amplification to the initial activating trigger. C3b molecules generated by either the CP/LP or the AP C3-convertases bind fB, thus forming more AP C3-convertases and providing rapid amplification (1).

To generate the AP C3-convertase, factor B (fB) first associates with C3b in a Mg^{2+}-dependent manner, to form the pro-convertase C3bB. In the presence of the serum protease factor D (fD), fB is cleaved and the N-terminal Ba fragment is released from the C3bB complex, creating the active AP C3-convertase (2).

Interaction sites in both C3b and fB have been delineated using different approaches. The α′NT and C345C domains in C3b include putative binding sites for fB required for C3 convertase formation (3-5). Both the α′NT and C345C domains are located in a part of the C3 molecule that undergoes large rearrangements upon activation of C3 into C3b, which explains why C3 does not interact with factor B (6). Similarly, structural analyses have suggested that formation of the AP C3-convertase probably depends on the structure and orientation of the CUB domain of C3b and that the interaction between C3b and fB is independent of the TED domain (7).

Factor B is composed of five structural domains. Three short consensus repeats (SCRs) at the N-terminus comprise the Ba fragment, whereas the large Bb fragment at the C-

terminus is comprised of a von Willebrand type A (vWA) domain followed by a serine-protease (SP) domain. Mutagenesis analyses of fB and functional characterization of rare mutations and common polymorphims associated with diseases involving complement dysregulation have suggested regions in the fB molecule that are crucial for the interaction with C3b (8-11). Thus, a number of fB residues near the Mg^{2+}-dependent metal ion-dependent adhesion site (MIDAS), including D279 (all amino acids are numbered to include the 25 aa-long signal peptide), in the vWA domain have been shown to influence the initial recognition of C3b by fB and the stability of the AP C3-convertase C3bBb (8-11). Mutagenesis studies have shown that the fB vWA α1 helix also contributes to the C3b-binding region of the fB vWA domain, whilst the fB vWA α4/5 helix region is somewhat removed from the C3b-binding region and more likely is involved in the binding site recognized by the complement regulators DAF and CR1 in C3bBb (12).

Formation of the C3bB complex also involves contact with the Ba domain (13). Using mutagenesis, antibody blocking and surface plasmon resonance methods it has been shown that both the triad of SCR domains (14-16) and an 8-aa long unstructured fragment at the amino terminus of the Ba fragment (17) provide important binding sites for C3b.

The crystal structure of human fB, recently resolved at 2.3Å resolution, demonstrated that the Ba domain was not extended but folded back onto the Bb domain. SCR2 and SCR3 of Ba were packed tightly into an antiparallel dimer capped by SCR1 (6). These structural data also indicate that SCR1 probably hinders access of the ligand C3b to the MIDAS of the vWA domain and that the triad of SCR domains is probably only weakly associated with the vWA and SP domains. Most interestingly, comparison of the factor B pro-enzyme (18) and the Bb fragment (19) structures, suggests that fB undergoes conformational changes upon binding to C3b, displacing the helix αL from its binding groove in the vWA domain and

exposing the long linker domain between the SCR3 and the vWA domains of fB that contains the scissile bond cleaved by fD (7, 18, 19).

Here, we sought to elucidate the structure of AP pro-convertase C3bB. To this end we have generated stable C3bB complexes in the presence of Ni^{2+}, purified them and determined their 3D structure at ~27 Å resolution using electron microscopy (EM). We also report structural analysis of the AP convertase C3bBb using the fB mutant D279G. These studies have revealed the architecture of the C3bB and C3bBb complexes providing key insights into the initial stages of the AP C3-convertase formation, its activation by fD, and fundamental aspects of its regulation.

Results and Discussion

Electron microscopy of C3b and C3bB(Ni^{2+}) complexes reveals that fB binds near the C345C domain in C3b.

The Ni^{2+} cation was used instead of Mg^{2+} to promote a stable C3bB(Ni^{2+}) complex that is otherwise undistinguishable from the physiological C3bB(Mg^{2+}) pro-convertase (8, 20, 21). Briefly, purified C3b and fB were mixed at 1:2 molar excess of fB in the presence of 5 mM $NiCl_2$. Subsequently, the C3bB(Ni^{2+}) complex was purified by gel filtration chromatography (SI Fig. S1; SI Materials and Methods) and fresh fractions containing C3bB(Ni^{2+}) were applied to carbon-coated EM grids and observed by electron microscopy (EM) after staining. Images from individual molecules were clearly detected in the EM fields (SI Fig. S2),these were extracted and reference-free 2D averages were obtained using EMAN (22) and maximum likelihood analysis (23). Averages of C3b were clearly evocative of the typical structure of C3b (Fig. 1A), whereas those of the complex were clearly larger, indicating the presence of an additional component bound to C3b (Fig. 1B). C3bB(Ni^{2+})

averages revealed views of the complex with an abundance of distinct shapes (Fig. 1B), indicating that it has likely bound to the support film in many different orientations representing rotations along its longitudinal axis. This assumption was confirmed later when performing the 3D reconstruction of the complex (see below). By contrast, single C3b molecule averages complied with a predominant orientation, probably due to the 'flat' nature of its structure (24, 25).

Images from single C3b molecules and the C3bB(Ni^{2+}) complex were processed using angular refinement methods to reconstruct their 3D structures. For each sample, we performed two independent experiments using as initial template for refinement either a very low resolution (> 60 Å) density map obtained after filtering the atomic structure of C3b, or a featureless Gaussian blob after adding noise. In both refinements, identical 3D solutions were obtained, compatible with the reference-free averages, indicating the absence of a significant bias from the initial reference (SI Fig. S3). During refinement, we detected that the data set for the C3bB(Ni^{2+}) complex covered views of the complex in many different orientations, whereas a more limited range of views was obtained for the free C3b molecule. Therefore, we collected additional data for C3b after tilting the specimen holder to complete the range of views (see Methods for details).

The 3D structure of C3b obtained by EM at a resolution of ~27 Å is, within the limits of this resolution, virtually identical to the published crystal structures (24, 25) (Fig. 1C). These atomic coordinates can be unambiguously fitted using unbiased computational methods into our EM density, allowing a straightforward assignment of the different domains of the EM structure to specific domains of C3b. On the other hand, the C3bB(Ni^{2+}) complex at a similar resolution reveals significant additional mass located in the proximities of the C345C domain but contacting a broad area of C3b (Fig. 1D and 2A). The atomic structure of C3b was resolved within the EM structure of the C3bB(Ni^{2+}) complex by an exhaustive 6-

dimensional search looking for all its possible orientations with the EM map. C3b was readily located within the complex given its very characteristic shape (Fig. 1D).

Overall, these findings indicate that the C3bB(Ni^{2+}) complex presents a more globular shape than the single C3b molecule, which allows the complex to adopt different poses on the carbon-coated support film. Furthermore, the comparison between the 2D averages and the 3D structures of C3b and C3bB(Ni^{2+}) revealed that the two data sets were clearly distinct (Fig. 1A and 1B), confirming the homogeneity of both preparations and pinpointing the location of fB in the C3bB(Ni^{2+}) complex.

Open conformation of fB within the C3bB(Ni^{2+}) complex

We comprehensively analyzed the conformation of fB after binding to C3b. The density of the fitted C3b was subtracted from that of the C3bB(Ni^{2+}) complex to determine the region of the map that accounts for fB (Fig. 2A and 2B). fB in complex with C3b revealed a well defined V-shape density divided into a large and a small domain, notably distinct from the compact globular shape that represents the crystallized isolated fB when observed at a similar resolution (Fig. 2B). Such differences indicate that fB undergoes substantial conformational changes when binding to C3b, as previously suggested (18).

To analyze further the conformation of fB within the C3bB(Ni^{2+}) complex we performed several fitting experiments within the density assigned to fB. Since the crystal structure of full-length factor B, recently solved at 2.3Å resolution (PDB file 2OK5), could not account for the observed density, we divided the fB structure into two halves, one containing the three SCRs (amino acid 26 to 220) and the other including the vWA and the SP domains (amino acid 253 to 764). The linker between SCR3 and vWA, including the αL helix, was removed from the analysis since its conformation in our structure should be considerably different to that in the lock conformation of factor B, and we cannot model these

changes at the resolution of our EM maps. When the atomic structure of the vWA-SP half was resolved within the whole density of fB in the C3bB(Ni^{2+}) complex using computational methods, vWA-SP was unambiguously located at the larger EM domain (cross-correlation coefficient 0.76) (Fig. 2C) . In fact, this is the only region of the EM map with sufficient size to accommodate Bb and, as a consequence, the remaining small domain of the fB EM density must comprise the Ba fragment containing the N-terminal SCR1-3 domains (Fig. 2C). Given the flat shape of the vWA-SP region in the C3bB(Ni^{2+}) complex, these two domains were found to fit the EM structure in only two possible orientations, placing the SP and vWA domains at either end of the large EM domain respectively (SI Fig. S4). One of these two solutions was discarded since it placed the SCR1-3 domains in a location where connection to the vWA domain could not be achieved with the length of the linker between them. The atomic structure corresponding to this region of fB (Ba fragment) could only be fitted manually, placing its C-terminus in the proximity of the vWA N-terminus, to best accommodate to the EM density (Fig. 2C). Therefore, the proposed orientation of the SCR1-3 triad represents an informed approximation.

Mechanistic insights into the assembly of the C3bB pro-convertase

The proposed arrangement for the C3bB(Ni^{2+}) complex illustrates key events during formation of the C3bB pro-enzyme. Firstly, consistent with early biochemical data (13), it shows that the Ba and Bb fragments both interact with C3b (Fig. 2 and 3). Moreover, it reveals that the vWA domain interacts with C345C with the MIDAS facing towards C3b (Fig. 3A), which is also in agreement with previous data demonstrating that a number of fB residues near the MIDAS influence the initial recognition of C3b by fB and the stability of the AP C3-convertase (8-11). The putative C3b-interacting sites in the vWA are also located as expected within the C3bB structure. Thus, the fB vWA α1 helix, shown by mutagenesis to

contribute to the C3b-binding region of the fB vWA domain (12), faces the interface with C3b, whereas the vWA α4/5 helix, not implicated in the interaction and more likely involved in the binding site recognized by the complement regulators DAF and CR1, faces away from the complex (Fig. 3A).

Most important is the distortion in conformation of fB bound to C3b in the C3bB(Ni^{2+}) complex compared to that recently reported for isolated fB (18). In the C3b-bound fB, the vWA-SP tandem is maintained as a unit, whereas the SCR1-3 region is displaced, likely interacting with the α'NT and CUB domains of C3b (Fig. 3B). This C3b-bound fB conformation supports the proposed model for the activation of fB, which suggests that upon binding to C3b the three SCRs of fB dislocate from the vWA and SP domains to allow access of the vWA domain to C3b (7, 18). The data also demonstrate contact points between the N-terminal region of Ba and the α'NT domain of C3b and between the Ba SCR2/3 and the CUB domain, in agreement with early mutagenesis, antibody blocking and surface plasmon resonance experiments (14-17).

The proposed C3bB structure validates the hypothesis that the large conformational rearrangements of fB upon interaction with C3b expose the flexible linker between the vWA and SCR3 domains that contains the site cleaved by factor D. This conformational change implies a major displacement of the SCR1-3 triad. Such a movement is certainly possible given the long and flexible linker (residues 221-252) connecting SCR3 with the vWA domain, only some of which is evident in the electron density of the published atomic structure of factor B (18). This linker must be cleaved between residues 259 and 260 by factor D to release the Ba fragment (26-259) in order to form the active convertase. Our model would place this cleavage point in the region connecting the two sides of the open conformation of fB in the C3bB complex. It is, therefore, quite exposed and potentially accessible to factor D.

It has been hypothesized that dislocation of the SCRs from the vWA and SP domains may be coupled, through the short SCR3-αL connecting loop, to the displacement of helix αL from its binding groove in the vWA domain. This, in turn, may induce the vWA and SP domains to adopt a conformation more closely resembling that of the active Bb fragment (18). Therefore, we tested whether the atomic structure of the active Bb fragment, where the vWA domain is rotated with respect to the SP domain (18), fitted better into the fB EM density in our structure of the C3bB complex. However, whilst the atomic structure of the activated Bb fragment also adequately fitted the EM structure, the differences in cross-correlation coefficients between the two "Bb" fits were not sufficient to allow a computational discrimination between the models (data not shown).

3D structure of the active C3bBb complex

In order to support our model for the C3bB(Ni^{2+}) complex, we generated a stable active C3bBb convertase. We used in this case the fB-D279G mutant because Ni^{2+} does not stabilizes the active enzyme to the same extent as the pro-enzyme. The fB-D279G mutant promotes high-affinity C3b-binding and it is correctly cleaved by factor D in the C3bB proenzyme to generate a very stable, functionally-active, AP convertase C3bBb (8, 11, 12) (SI Materials and Methods). The $C3bBb_{279G}$ complex was purified by gel filtration (SI Fig. S5) and analyzed by EM in a similar way to the C3bB(Ni^{2+}) complex. Intriguingly, some 2D averages of C3bBb revealed lobes of density projecting out from the C3b structure; we later ascribed these to the C345C, vWA and SP domains (Fig. 4A). Some of these 2D averages are very similar to the EM images of a AP convertase generated with fB-WT reported earlier by Smith et al. (26) suggesting that the SP domain projects out from the convertase.

3D reconstruction analyses showed that the active convertase lacked the small domain of fB in the C3bB complex that we had ascribed to the Ba fragment (Fig. 4B), fully

supporting our structural model. Interestingly, during the 3D refinement we observed that the density accounting for the SP domain was spread out along a range of possible conformations, reducing its average density in the 3D reconstruction (Fig. 4B). Reference-free 2D averages of the EM data revealed that whereas some averages shown a defined three-dot pattern (Fig. 4C, i), most side views of C3bBb demonstrated a well defined C3b molecule with an indistinct density for the projecting Bb region (Fig. 4C, ii). Such blurring suggests that the conformation of the vWA-SP domains is flexible, likely due to the absence of additional interaction points provided by the Ba SCR triad. In addition, the C3bBb structure shows that the SP domain of fB projects from the structure without contacting C3b and makes the catalytic site accessible to its substrate. Whether this difference between C3bB and C3bBb regarding the position of the SP domain is a consequence of conformational changes within the Bb fragment after the release of the Ba fragment cannot be solved at the resolution provide by our studies.

Functional implications of the 3D structures of C3bB(Ni^{2+}) and C3bBb regarding decay acceleration mediated by DAF, CR1 and fH.

The AP C3 convertase plays a central role in the amplification of complement cascade and for this reason its activity is strictly regulated. This regulation is achieved by modulating the stability of the AP C3–convertase, which localize complement amplification to the surface of the pathogens and prevents unspecific damage to self-tissues. Complement regulatory proteins either stabilize the C3bBb complex (Properdin) or accelerate its decay (factor H (fH), decay accelerating factor (DAF) or complement receptor 1 (CR1)). The C3bB and C3bBb EM structures described here shed new light on the mechanisms underlying the decay acceleration mediated by DAF, CR1 and fH.

In DAF, the functional activity is located within four SCR domains at the N-terminus. Using surface plasmon resonance it has been shown that DAF mediates decay of the C3bBb convertase, but not of the proenzyme, C3bB, and the major site of interaction is within the Bb

fragment (27). Using truncated recombinant DAF molecules it has been demonstrated that DAF-SCR2 interacts with Bb, whereas DAF-SCR4 interacts with C3b. These data suggest that DAF interacts with C3bBb through major sites in SCR2 and SCR4. It has been suggested that the high affinity of binding to Bb via SCR2 (compared to little or no binding to fB), concentrates DAF on the active convertase, whereas the weaker interactions through SCR4 with C3b directly mediate decay acceleration (28).

We have already discussed that the fB vWA α4/5 helix region is exposed in our structure (Fig. 3) and that mutagenesis data highlight this helix region as a binding site recognized by DAF and CR1 (12). We recently described a novel fB mutation, K323E, in a patient with atypical hemolytic uremic syndrome (aHUS) that makes the C3bBb convertase resistant to decay by DAF and fH (11). This mutation, located in close proximity to the α4/5 helix region of the vWA domain (Fig. 3), is remarkable because it neither modifies the formation rate of the C3bB and C3bBb complexes, nor their spontaneous decay, suggesting that the mutation specifically affects the binding site in the vWA domain for the complement regulators DAF and fH (11).

The C3bB and C3bBb EM structures described here support the concept of two binding sites for DAF in the C3bBb complex, one located on the surface of the vWA domain in Bb, away from the interaction surface with C3b (DAF-SCR2), and the other in C3b in the region that is occupied by the Ba fragment in the C3bB pro-convertase (DAF-SCR4). This readily explains the requirement for Ba removal from the C3bB complex in order that DAF can bind and mediate efficient decay acceleration.

Concluding remarks

The alternative pathway (AP) C3-convertase is an unstable bimolecular complex formed by C3b and factor B that plays a crucial role within the complement cascade as it

provides the exponential amplification to the initial activating trigger. Assembly and regulation of the AP C3 convertase is exquisitely modulated to make possible the elimination of foreign agents by effector cells while at the same time protecting self-tissues from complement-mediated destruction. In fact, alterations in its formation rate, its stability or its regulation result in AP complement dysregulation leading to infectious diseases or tissue damage (29). Understanding how the AP convertase is assembled and regulated is, therefore, essential. Here we present in 3D the conformational transitions of fB following binding to C3b and formation of the AP pro-enzyme. Importantly, we demonstrate that binding to C3b promotes an opening of the fB conformation by displacing the SCR1-3 region (Ba fragment) from the SP-vWA tandem (Bb fragment). This open conformation of fB exposes the linker connecting the Bb and Ba fragments, permitting its cleavage by fD. Interestingly, the conformation of Bb in the active convertase reveals some degree of flexibility, with the SP domain adopting various conformations with respect to C3b. Our model also reveals important aspects of the regulation of the AP C3 convertase by DAF and perhaps other complement regulators like fH and CR1. These data will aid to explore the potential of the AP C3 convertase as a therapeutic target in the development of inhibitors to prevent or reduce tissue damage caused by dysregulated complement activation. Most importantly, our model provides a structural framework onto which other proteins of considerable interest in the pathophysiology of the AP convertase, like properdin or C3Nef, can be easily modelled. The methodology used in this work, single particle electron microscopy, in combination with crystallography offers a powerful tool to dissect protein interactions underlying the activity and regulation of this remarkable protein complex, the AP C3 convertase.

Materials and Methods

Electron microscopy and 3D reconstruction

Purified C3b, C3bB(Ni^{2+}) or C3bBb complexes in 25mM TrisHCl pH8.0, 50mM NaCl were applied to carbon-coated grids and negatively stained with 1% uranyl formate. The molecular weight of these complexes (~200kDa) did not allow their detection without staining. Observations were performed in a JEOL 1230 electron microscope operated at 100kV and micrographs were recorded at a nominal magnification of 50,000 under low dose conditions. Micrographs were digitized and averaged to 4.2 Å/pixel and the contrast transfer function estimated using CTFFIND3 (30) and corrected by flipping phases. Around 6000 images of molecules for each specimen were extracted and refined using EMAN (22). Reference-free averages were obtained using EMAN and maximum likelihood (23). We used two different starting 3D templates for refinement in two independent experiments. Identical results were obtained with either initial reference (SI Fig. S3), substantiating the final reconstruction and the absence of bias during the refinement. One reference was built by low-pass filtering the atomic structure of C3b (PDB file 2i07) to very low resolution (> 60 Å) whereas a second template was a featureless noisy Gaussian blob (SI Fig. S3). Images collected for the C3bB(Ni^{2+}) and C3bBb complexes revealed adequate Euler angles coverage. On the other hand, images of C3b mostly corresponded to tilting angles around an abundant front view, consistent with the flat appearance of C3b. In order to increase this angular coverage, micrographs were also taken after tilting the specimen holder at 20 and 35 degrees, and the images were added to the data set collected without tilting. The resolution of the maps was estimated to be ~28 Å, ~27 Å and ~28 Å for C3b, C3bB(Ni^{2+}) and C3bBb respectively by Fourier Shell Correlation using the criteria of a correlation coefficient of 0.5. The absolute handedness of the reconstruction was defined by comparison with the atomic structure of C3b.

Fitting of the atomic structures into the EM maps

We performed a rigid-body fit of C3b (PDB file 2i07) into the EM reconstruction of C3b and the C3bB(Ni^{2+}) complex using ADP_EM (31). C3b was unambiguously located in the C3bB(Ni^{2+}) complex and a difference map between this fitted C3b and the full map was used to extract the density in the complex assigned to fB. The VWA and SP domains of fB (PDB file 2OK5) (18) were fitted as a rigid-body into this difference map using ADP_EM without any a priori assumption. Only one solution was compatible with the polypeptide backbone linking SCR3 to the vWA domain, this solution was then selected. The Ba fragment corresponding to the SCR1-3 trimer was manually fitted in the remaining density.

Acknowledgements

This work has been supported by projects SAF2005-00775 (OL), SAF2008-00451 (OL), SAF2005-0913 and SAF2008-00226 (SRC) from the Spanish Ministry of Science, CAM S-BIO-0214-2006 (OL) from the Autonomous Region of Madrid and RD06/0020/1001 (OL) of the "Red Temática Investigación Cooperativa en Cáncer (RTICC)" from the "Instituto Carlos III". OL group is additionally supported by the Human Frontiers Science Program (RGP39/2008). SRC group is additionally supported by CIBERER (INTRA/08/738.2) and the Fundacion Renal Iñigo Alvarez de Toledo. We are very grateful to B.P. Morgan and C. Harris for their long-term collaborative support of our work and their comments on the manuscript. We are also indebted to Elena Goicoechea de Jorge and Ernesto Arias-Palomo for his help.

The EM map of C3bB(Ni^{2+}) complex has been deposited in the 3D EM database (http://www.ebi.ac.uk/msd/) under accession code EMD-1583.

References

1. Volanakis JE (1998) *The Human Complement System in Health and Disease* (Marcel Dekker, Inc., New York) 10th Ed pp 9-32.
2. Pangburn MK & Muller-Eberhard HJ (1986) The C3 convertase of the alternative pathway of human complement. Enzymic properties of the bimolecular proteinase. *Biochem J* 235(3):723-730.
3. Taniguchi-Sidle A & Isenman DE (1994) Interactions of human complement component C3 with factor B and with complement receptors type 1 (CR1, CD35) and type 3 (CR3, CD11b/CD18) involve an acidic sequence at the N-terminus of C3 α-chain. *J Immunol* 153(11):5285-5302.
4. Kölln J, Bredehorst R, & Spillner E (2005) Engineering of human complement component C3 for catalytic inhibition of complement. *Immunol Lett* 98(1):49-56.
5. Kölln J, Spillner E, Andra J, Klensang K, & Bredehorst R (2004) Complement inactivation by recombinant human C3 derivatives. *J Immunol* 173(9):5540-5545.
6. Janssen BJC & Gros P (2007) Structural insights into the central complement component C3. *Mol Immunol* 44(1-3):3-10.
7. Gros P, Milder FJ, & Janssen BJC (2008) Complement driven by conformational changes. *Nature Rev Immunol* 8(1):48-58.
8. Hourcade DE, Mitchell LM, & Oglesby TJ (1999) Mutations of the type A domain of complement factor B that promote high- affinity C3b-binding. *J Immunol* 162(5):2906-2911.
9. Tuckwell DS, Xu Y, Newham P, Humphries MJ, & Volanakis JE (1997) Surface loops adjacent to the cation-binding site of the complement factor B von Willebrand factor type A module determine C3b binding specificity. *Biochemistry* 36(22):6605-6613.
10. Hinshelwood J, Spencer DIR, Edwards YJK, & Perkins SJ (1999) Identification of the C3b binding site in a recombinant vWF-A domain of complement factor B by surface-enhanced laser desorption-ionisation affinity mass spectrometry and homology modelling: Implications for the activity of factor B. *J Mol Biol* 294(2):587-599.

11. Goicoechea De Jorge E*, et al.* (2007) Gain-of-function mutations in complement factor B are associated with atypical hemolytic uremic syndrome. *Proc Natl Acad Sci USA* 104(1):240-245.

12. Hourcade DE, Mitchell L, Kuttner-Kondo LA, Atkinson JP, & Edward Medof M (2002) Decay-accelerating factor (DAF), complement receptor 1 (CR1), and factor H dissociate the complement AP C3 convertase (C3bBb) via sites on the type A domain of Bb. *J Biol Chem* 277(2):1107-1112.

13. Pryzdial ELG & Isenman DE (1987) Alternative complement pathway activation fragment Ba binds to C3b. *J Biol Chem.* 262(4):1519-1525.

14. Hourcade DE, Wagner LM, & Oglesby TJ (1995) Analysis of the short consensus repeats of human complement factor B by site-directed mutagenesis. *J Biol Chem* 270(34):19716-19722.

15. Xu Y & Volanakis JE (1997) Contribution of the Complement Control Protein Modules of C2 in C4b Binding Assessed by Analysis of C2/Factor B Chimeras. *J Immunol* 158(12):5958-5965.

16. Thurman JM*, et al.* (2005) A novel inhibitor of the alternative complement pathway prevents antiphospholipid antibody-induced pregnancy loss in mice. *Mol Immunol* 42(1):87-97.

17. Montes T*, et al.* (2008) Functional differences between common factor B polymorphic variants: An explanation for association with AMD. *Mol Immunol* 45:4098.

18. Milder FJ*, et al.* (2007) Factor B structure provides insights into activation of the central protease of the complement system. *Nature Struct Mol Biol* 14(3):224-228.

19. Ponnuraj K*, et al.* (2004) Structural analysis of engineered Bb fragment of complement factor B: Insights into the activation mechanism of the alternative pathway C3-convertase. *Mol Cell* 14(1):17-28.

20. Hourcade DE, Mitchell LM, & Oglesby TJ (1998) A conserved element in the serine protease domain of complement factor B. *J Biol Chem* 273(40):25996-26000.

21. Fishelson Z & Muller-Eberhard HJ (1984) Residual hemolytic and proteolytic activity expressed by Bb after decay-dissociation of C3b,Bb. *J Immunol* 132(3):1425-1429.

22. Ludtke SJ, Baldwin PR, & Chiu W (1999) EMAN: Semiautomated software for high-resolution single-particle reconstructions. *J Struct Biol* 128(1):82-97.

23. Scheres SHW, Valle M, & Carazo JM (2005) Fast maximum-likelihood refinement of electron microscopy images. *Bioinformatics* 21(SUPPL. 2):ii243-ii244.

24. Janssen BJC*, et al.* (2005) Structures of complement component C3 provide insights into the function and evolution of immunity. *Nature* 437(7058):505-511.

25. Wiesmann C*, et al.* (2006) Structure of C3b in complex with CRIg gives insights into regulation of complement activation. *Nature* 444(7116):217-220.

26. Smith CA, Vogel CW, & Muller Eberhard HJ (1984) MHC class III products: An electron microscopic study of the C3 convertases of human complement. *J Exp Med* 159(1):324-329.

27. Harris CL, Abbott RJM, Smith RA, Morgan BP, & Lea SM (2005) Molecular dissection of interactions between components of the alternative pathway of complement and decay accelerating factor (CD55). *J Biol Chem* 280(4):2569-2578.

28. Harris CL, Pettigrew DM, Lea SM, & Morgan BP (2007) Decay-accelerating factor must bind both components of the complement alternative pathway C3 convertase to mediate efficient decay. *J Immunol* 178(1):352-359.

29. Holers VM (2008) The spectrum of complement alternative pathway-mediated diseases. *Immunol Rev* 223(1):300-316.

30. Mindell JA & Grigorieff N (2003) Accurate determination of local defocus and specimen tilt in electron microscopy. *J Struct Biol* 142(3):334-347.

31. Garzón JI, Kovacs J, Abagyan R, & Chacón P (2007) ADP_EM: Fast exhaustive multi-resolution docking for high-throughput coverage. *Bioinformatics* 23(4):427-433.

Figure Legends

Figure 1. **Electron microscopy and 3D reconstruction of C3b and C3bB(Ni^{2+})**

(A) Reference-free 2D averages obtained for the data set containing images of single molecules of C3b. These averages reveal a characteristic “L” shape evocative of the C3b crystal structure. (B) Reference-free 2D averages of C3bB(Ni^{2+}) display a bulky appearance

compatible with fB binding to C3b. (C) Front view of the 3D structure of C3b derived from the EM data at a resolution of 28 Å (gray density). The atomic structure of C3b (PDB file 2i07) has been fitted within the EM map and displayed in purple with the C345C and CUB domains highlighted in orange and blue respectively. (D) Several views of the 3D structure of C3bB(Ni^{2+}) at 27 Å resolution (gray density). Fitting of the atomic structure of C3b (PDB file 2i07) allows the assignment of specific regions of the EM map to specific C3b domains. Some densities of the 3D reconstruction cannot be accounted by C3b (labeled as asterisks), and correspond to C3b-bound fB.

Figure 2. **Open conformation of fB within the C3bB(Ni^{2+}) complex**

(A) Views of the 3D reconstruction of C3bB(Ni^{2+}). C3b in the complex has been colored in orange whereas fB is shown in green. (B) The structure of inactive fB (PDB file 2OK5) shows a compact conformation (left panels). This structure was filtered to ~25 Å resolution and was compared with the EM reconstruction (top left panel). C3b-bound fB was extracted by calculating the difference map between the EM density for C3bB(Ni^{2+}) and the fitted atomic structure of C3b (right panel), and was found to display a more open conformation. SP, vWA and SCR1-3 domains have been colored in pale blue, green and yellow respectively. (C) Fitting of the atomic structure of fB into the structure of C3bB(Ni^{2+}) complex. fB structure was divided in two segments corresponding to Bb and Ba fragments, and fitted separately within the density assigned to fB in the complex.

Figure 3. **Structural insights in the assembling of the pro-convertase**

(A) Representation of an atomic model for fB within the C3bB(Ni^{2+}) complex. For clarity only the C345C domain of C3b is represented. Color codes for domains as in Fig. 2. Specific residues have been highlighted representing them as space-filled amino acids. These include D279 (known to affect pro-enzyme formation), K323 (known to affect regulation by DAF) and Q34 (to label the N-terminus of the Ba fragment). The vWA α1 helix (contributing to the

C3b-binding region) and vWA α4/5 helix (implicated in the DAF/CR1 binding site) are highlighted in blue and red ribbons, respectively. The N-terminus of the C3b α' chain (α'NT) is depicted with space-filled amino acids. (B) A side view of the structural model of the C3bB(Ni^{2+}) complex where the atomic structure of C3b (PDB file 2i07) is also represented in purple color. Color codes as in Fig. 1 and 2.

Figure 4. **3D structure of the C3bBb convertase**

(A) A reference-free 2D average corresponding to a side view of the C3bBb complex where the vWA and SP domains appear projecting from the C3b structure. (B) Two views of the C3bBb complex revealing that the density assigned to the SCR1-3 domains in the structure of C3bB(Ni^{2+}) is missing. This reconstruction represents a 3D average where the density of the SP domain is blurred due to conformational flexibility. (C) The flexibility of the vWA-SP cassette projecting from the C3bBb complex is reflected in the 2D reference-free averages of the data. Whereas some averages show a good definition of 3 dots of density corresponding to the C345C, vWA and SP domains (i), others reveal some blurring of this area (ii) whist maintaining the definition of the C3b molecule.

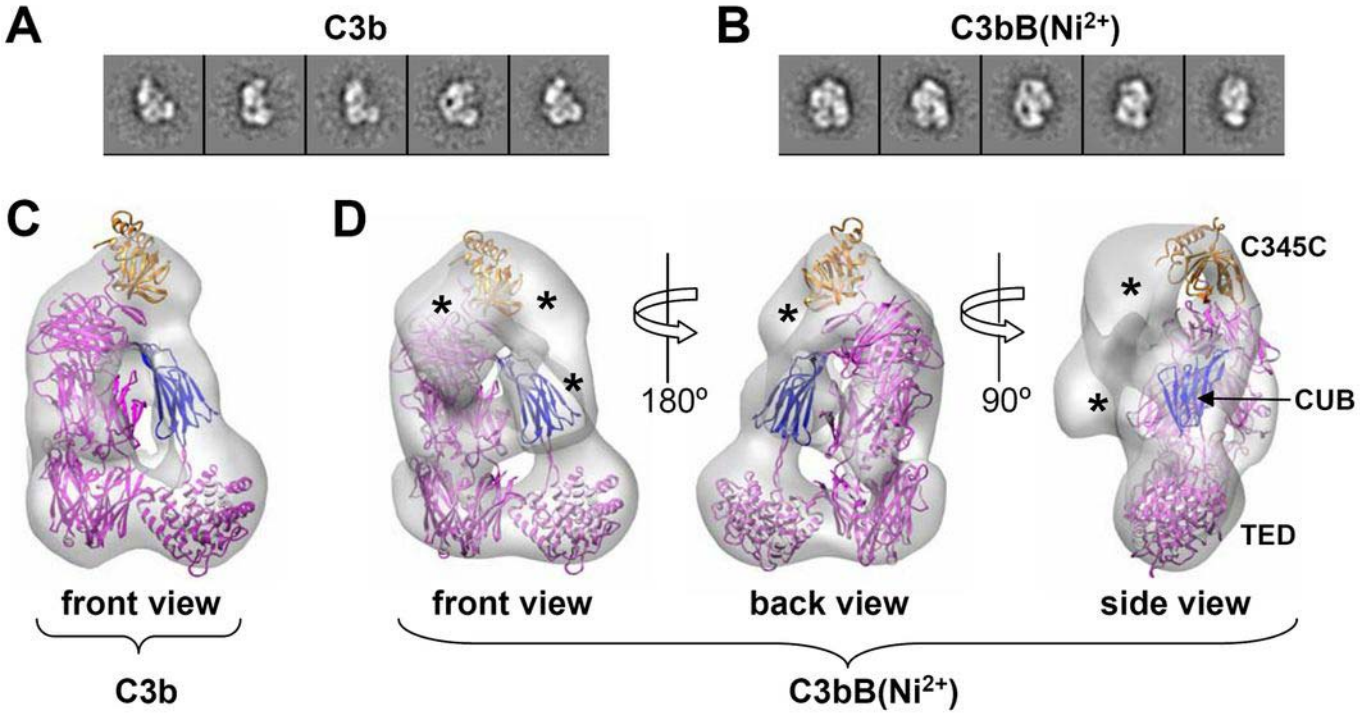
A
C3b
B
C3bB(Ni2+)
C
D
180°
90°
C345C
CUB
TED
front view
front view
back view
side view
C3b
C3bB(Ni2+)

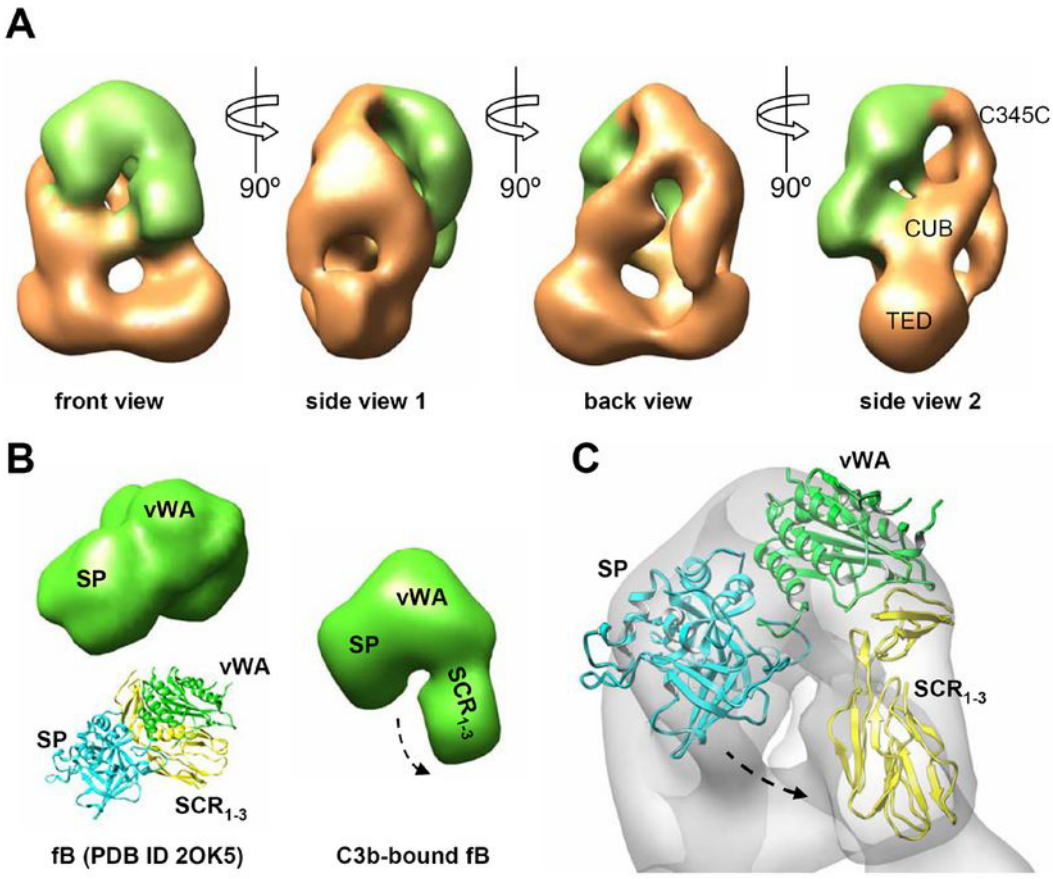
A
90°
90°
90°
C345C
CUB
TED
front view
side view 1
back view
side view 2
B
vWA
SP
vWA
SP
SCR1-3
fB (PDB ID 2OK5)
vWA
SP
SCR1-3
C3b-bound fB
C
vWA
SP
SCR1-3

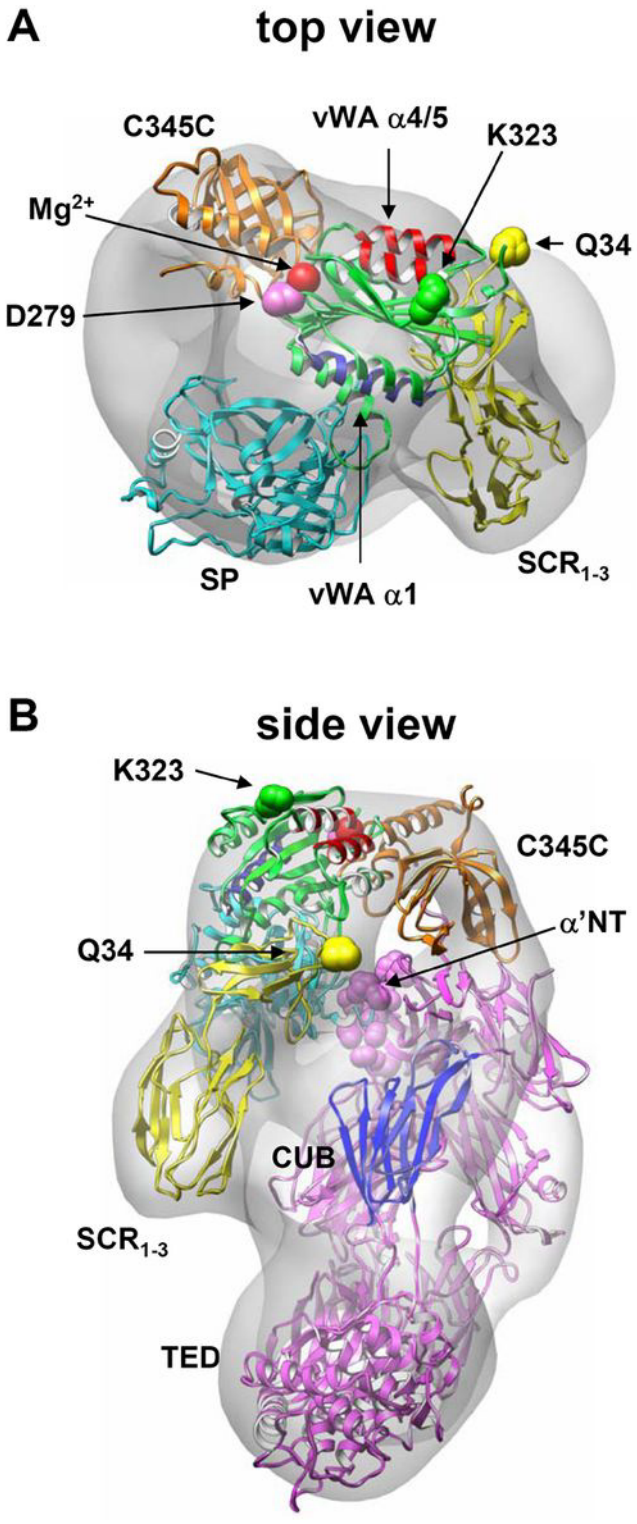
A
top view
C345C
vWA α4/5
K323
Mg2+
Q34
D279
SP
vWA α1
SCR1-3
B
side view
K323
C345C
α'NT
Q34
CUB
SCR1-3
TED

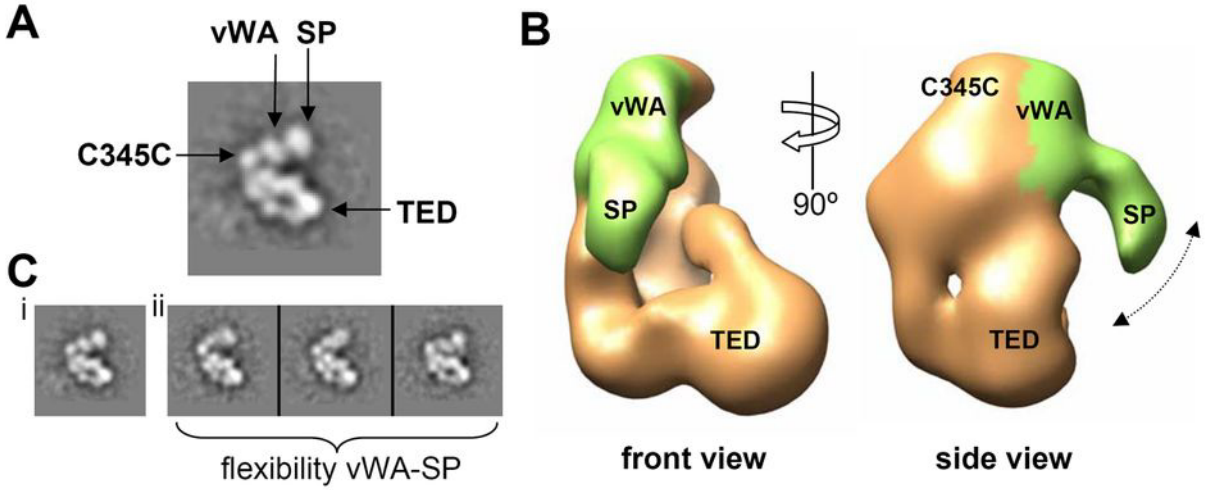
A
vWA
SP
C345C
TED
C
i
ii
flexibility vWA-SP
B
vWA
SP
TED
90°
C345C
vWA
SP
TED
front view
side view

Supplementary Materials and Methods

Preparation of the complement C3b fragment.

C3 was prepared from pooled normal human plasma. Plasma was subjected to a 4-12% cut with PEG4000, the pellet was solubilized in 10mM Na/K phosphate pH7.6, 5mM NaCl and applied to a DEAE-Sepharose anion exchange column attached to an Akta Prime system (GE Healthcare, Amersham, UK). Protein was fractionated using a gradient to 0.5M NaCl, C3-containing fractions were identified by SDS-PAGE, dialyzed against 20mM Na/K phosphate pH6, 60mM NaCl and applied to a Source S cation exchange column (GE Healthcare). Protein was eluted with a gradient to 0.5M NaCl. C3-containing fractions were pooled and concentrated. C3b was generated by limited digestion with trypsin as previously described (Sánchez-Corral P, et al. (1989) Separation of active and inactive forms of the third component of human complement, C3, by fast protein liquid chromatography (FPLC). J Immunol Methods 122(1):105-113.) and re-purified by gel filtration on a SuperoseTM 6 10/300 column (GE Healthcare). C3b was obtained without any detectable contaminants or aggregates (Supplementary Figure 1A).

Production and purification of recombinant fB

The D279G amino acid substitution was introduced in the fB cDNA by using QuickChange site-directed mutagenesis kit (Stratagene, La Jolla, CA) and appropriate primers. Both cDNAs encoding full length fB-WT and fB-D279G were introduced in the eukaryote expression vector pCI-Neo (Promega, Madison, WI) and the resulting clones entirely sequenced to confirm a correct DNA sequence. CHO cells were maintained in Ham-F12 medium (GIBCO-BRL, Carlsbad, CA) supplemented with 10% fetal calf serum, L-glutamine (2 mM final concentration), penicillin and streptomycin (10 U/ml and 100 μg/ml). The neomycin analogue, G418 sulfate (Geneticin; GIBCO-BRL, Carlsbad, CA), at 500

μg/mL, was used for selection of transfected cells. fB-cDNA transfections were performed using Lipofectine (Invitrogen) as recommended by the manufacturer. Cells were plated in p60 plates 1 day prior to transfection at 5 x 105 cells per well. Transfections were carried out with 10 μg of the pCI-Neo constructs and 24 μl of Lipofectine in a total volume of 1 ml of medium per well. Stable transfected CHO cells were cloned by limiting dilution and clones producing the highest levels of fB (fB-WT 20μg/ml; fB-D279G 2μg/ml) were expanded for production. fB concentration was quantified by ELISA as previously described (11). The recombinant fBs were purified from tissue culture supernatant by affinity chromatography using the JC1 monoclonal antibody (anti-human Bb, a gift from Prof. B.P. Morgan, Cardiff, UK) coupled to a HiTrap NHS-activated column according to the manufacturer's instructions (GE Healthcare). Bound fB was eluted with 0.1M Glycine/HCl pH 2.5, immediately neutralized with 2M Tris pH 8.6 and re-purified by gel filtration on a SuperoseTM 6 10/300 column (GE Healthcare). Both fB-WT and fB-D279G were obtained without any detectable contaminants or aggregates (Supplementary Figure 1A).

Generation and purification of C3bB complexes.

The Ni^{2+} cation was used instead of Mg^{2+} to promote a stable C3bB(Ni^{2+}) complex that is otherwise undistinguishable from the physiological C3bB(Mg^{2+}) pro-convertase. Purified C3b and fB were mixed in an (1:2) molar excess of fB in 20mM Tris, pH=7.6 buffer containing 50mM NaCl and either 20 mM EDTA or in 5mM $NiCl_2$ and allowed to interact for 15 at room temperature. Subsequently, both preparations were size-fractionated by gel filtration chromatography on a calibrated SuperoseTM 6 10/300 column (GE Healthcare) (Supplementary Figure 1B). In the absence of divalent cations (EDTA-sample), fB does not interact with C3b and both proteins elute separately from the Superose column as illustrated by the SDS-PAGE analysis of the corresponding fractions (Supplementary Figure 1C). In the presence of Ni^{2+} and a 1:2 molar excess of fB, C3b readily interacts with fB to form

C3bB(Ni^{2+}) complexes. SDS-PAGE characterization of the elution fractions from the Superose column illustrates the presence of the C3bB(Ni^{2+}) complex which elutes from the column in a single peak that precedes and partially overlaps the peak containing the single C3b molecules (Supplementary Figures 1B and 1C). To avoid a potential contamination of single C3b molecules in the fractions corresponding to the C3bB(Ni^{2+}) complex, samples for the EM analysis were collected exclusively from the initial elution fractions of the peak containing the C3bB(Ni^{2+}) complex.

Generation and purification of C3bBb complexes.

We have used the fB-D279G mutant instead of the fB-WT protein to promote a relatively stable active C3bBb convertase. For the generation of the C3bB complex, purified C3b and fB-D279G were mixed in an (1:2) molar excess of fB in 20mM Tris, pH=7.6 buffer containing 50mM NaCl and 5mM MgCl2 and were incubated for 15 minutes at room temperature. Subsequently, we added fD (Comptech. Inc., Tyler, USA) at a 1:500 molar ratio to fB, incubated for 1 minute at 37ºC and size-fractionated the mix by gel filtration chromatography on a calibrated SuperoseTM 6 10/300 column (GE Healthcare) (Supplementary Figure 4A). The presence of C3bBb complexes was demonstrated by SDS-PAGE analysis illustrating that, as expected, most of the Bb fragment eluted in the fractions containing the C3b molecule (Supplementary Figure 4B). The C3bBb complex eluted from the column in a single peak that significantly overlapped the peak containing the single C3b molecules (Supplementary Figures 4A and 4B). To minimize the contamination of single C3b molecules in the fractions corresponding to the C3bBb complex, samples for the EM analysis were collected exclusively from the initial elution fractions of the peak containing the C3bBb complex.

Legends to Supplementary Figures

Figure S1. **Purification of C3b, fB and the C3bB(Ni^{2+}) complex.**

(A) Purification of C3b and fB. Chromatograms from the final step of C3b and fB-WT purification on a Superose 6 10/300 gel filtration column. The Y-axis (milliabsorbance units, mAU) plots absorbance at 280 nm, the X-axis plots retention time in ml. Vertical lines indicate the fractions that were pooled for generating the C3bB(Ni^{2+}) complex and for the EM experiments. The Coomassie stained gel illustrates purity of the final C3b and fB preparations.

(B) Purification of the C3bB(Ni^{2+}) complexes. Elution profiles of the C3b-fB mix in the presence of 20mM EDTA (No complex formed; dotted line) or 5mM $NiCl_2$ (Complex formed; solid line) from the Superose 6 10/300 gel filtration column. The Y-axis (milliabsorbance units, mAU) plots absorbance at 280 nm, the X-axis plots number of fraction collected. Elution position for fB, C3b and the C3bB(Ni^{2+}) complex are indicated.

(C) Characterization of C3bB(Ni^{2+}) and complexes by SDS-PAGE. Fractions of the gel filtration chromatography experiments shown in (b) were analyzed by SDS-PAGE silver stained gels. The presence of the C3bB(Ni^{2+}) complex was clearly demonstrated in the presence of 5mM $NiCl_2$, as illustrated by the advanced elution position of fB (fractions 40-43), compared to that of the single fB molecules (fractions 45-48). Note that for the EM analysis of the C3bB(Ni^{2+}) complex only fractions 40 and 41 were used.

Figure S2. **Electron micrographs of C3b and C3bB(Ni^{2+})**

Selected field of an electron micrograph of C3b (a) and C3bB(Ni^{2+}) complex (b). Scale bar represents 100nm. Some representative images of individual molecules are indicated using arrows.

Figure S3. **Image processing of C3bB(Ni^{2+}) using angular refinement methods**

Angular refinement was performed in two independent experiments from two different volumes, either a low-pass filtered version of the atomic structure of C3b (a) or a random noisy Gaussian blob (b). Three views of the initial template in each case and of several output volumes along the progression of the refinement are shown. It can be noted that two very distantly related initial references converge into a similar 3D structure, indicating the absence of bias of the initial template during the refinement and the accuracy of the final reconstruction.

Figure S4. Output solutions after fitting the atomic structure of the vWA and the SP domains of fB (amino acids 253 to 764) into the EM density for fB extracted from the 3D structure of C3bB(Ni2+).

(A) List of the top 11 solutions automatically obtained in the fitting experiment using computational methods with their corresponding cross-correlation values for the comparison between the EM density and the atomic structures. The table includes an indication of whether the vWA-SP orientation was interpreted as compatible with the continuity of the polypeptide chain (labeled “OK”) or incompatible with this continuity (labeled “flip”). The figure also shows the correlation values for the first two fitting outputs (20 and 21) that are significantly different from the top 11 outputs.

(B) All the output solutions considered to be correct of the above list are practically identical and represented just slightly variations around a similar common output. These solutions are depicted as ribbons using a different color for each solution.

(C) Similarly, all “flipped” solutions were very similar and they are also represented as ribbons using different colors.

(D) The two outputs with low cross-correlation values are also color-coded.

Figure S5. **Purification of the C3bBb complex.**

(A) Purification of the C3bBb complexes. Elution profiles of the C3b / fB-D279G mix in the presence of 5mM $MgCl_2$ and fD (active convertase formed; solid line) and isolated C3b (dotted line) from the Superose 6 10/300 gel filtration column. The Y-axis (milliabsorbance units, mAU) plots absorbance at 280 nm, the X-axis plots number of fraction collected. Elution position for the Bb fragment, C3b and the C3bBb complex are indicated.

(B) Characterization of C3bBb complexes by SDS-PAGE. Fractions of the gel filtration chromatography experiments shown in (a) were analyzed by SDS-PAGE silver stained gels. The presence of the C3bBb complex was clearly demonstrated by the earlier elution of the Bb fragment (fractions 37-41), compared to that of the single Bb molecules (fractions 47-50). Only the initial fractions (38 and 39) of the C3bBb peak from gel filtration chromatography were used in the EM experiments to minimize the presence of single C3b molecules in the C3bBb preparations.

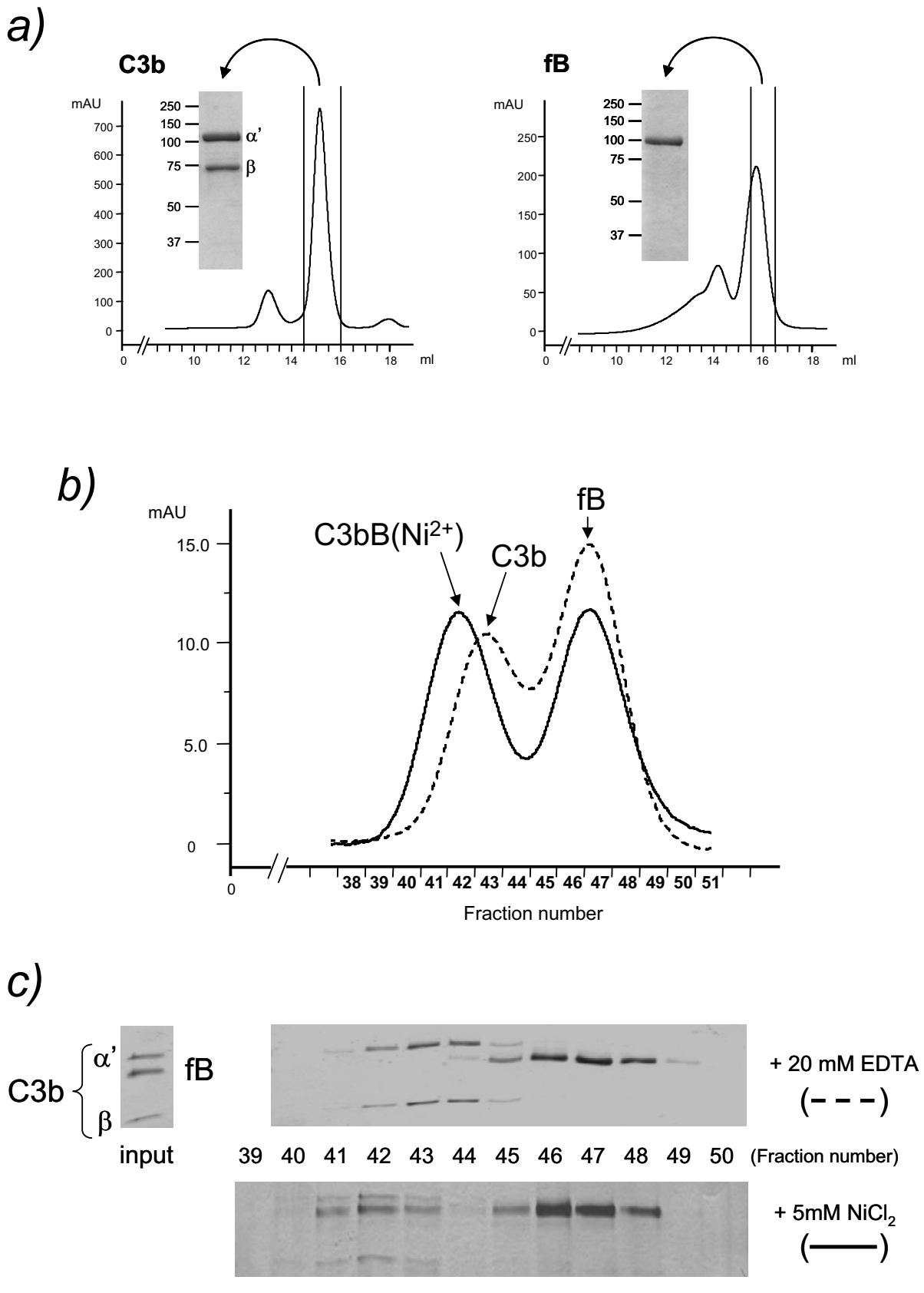
a)
C3b
fB
mAU
ml
α'
β
b)
C3bB(Ni2+)
C3b
fB
mAU
Fraction number
c)
C3b
α'
β
fB
input
39 40 41 42 43 44 45 46 47 48 49 50 (Fraction number)
+ 20 mM EDTA
(– – –)
+ 5mM NiCl2
(——)

a)

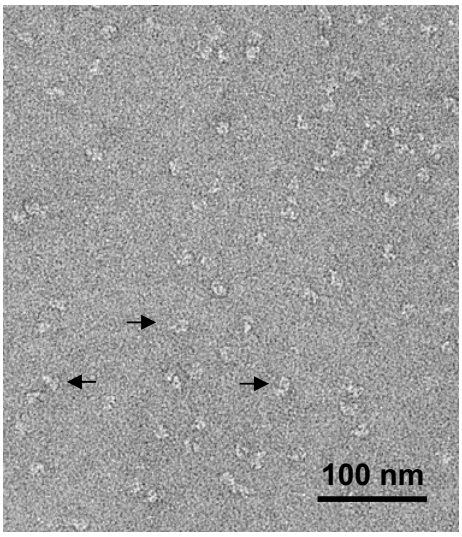

C3b

b)

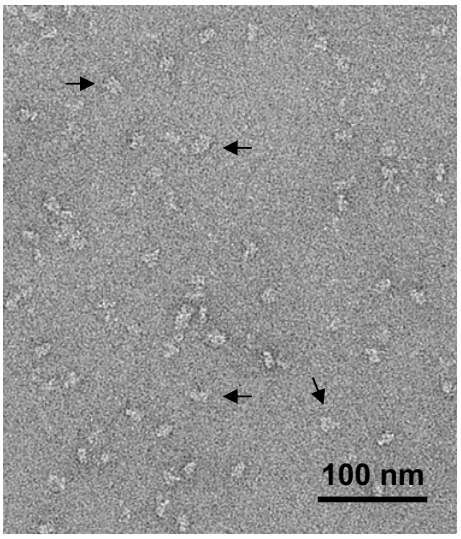

C3bB(Ni^{2+})

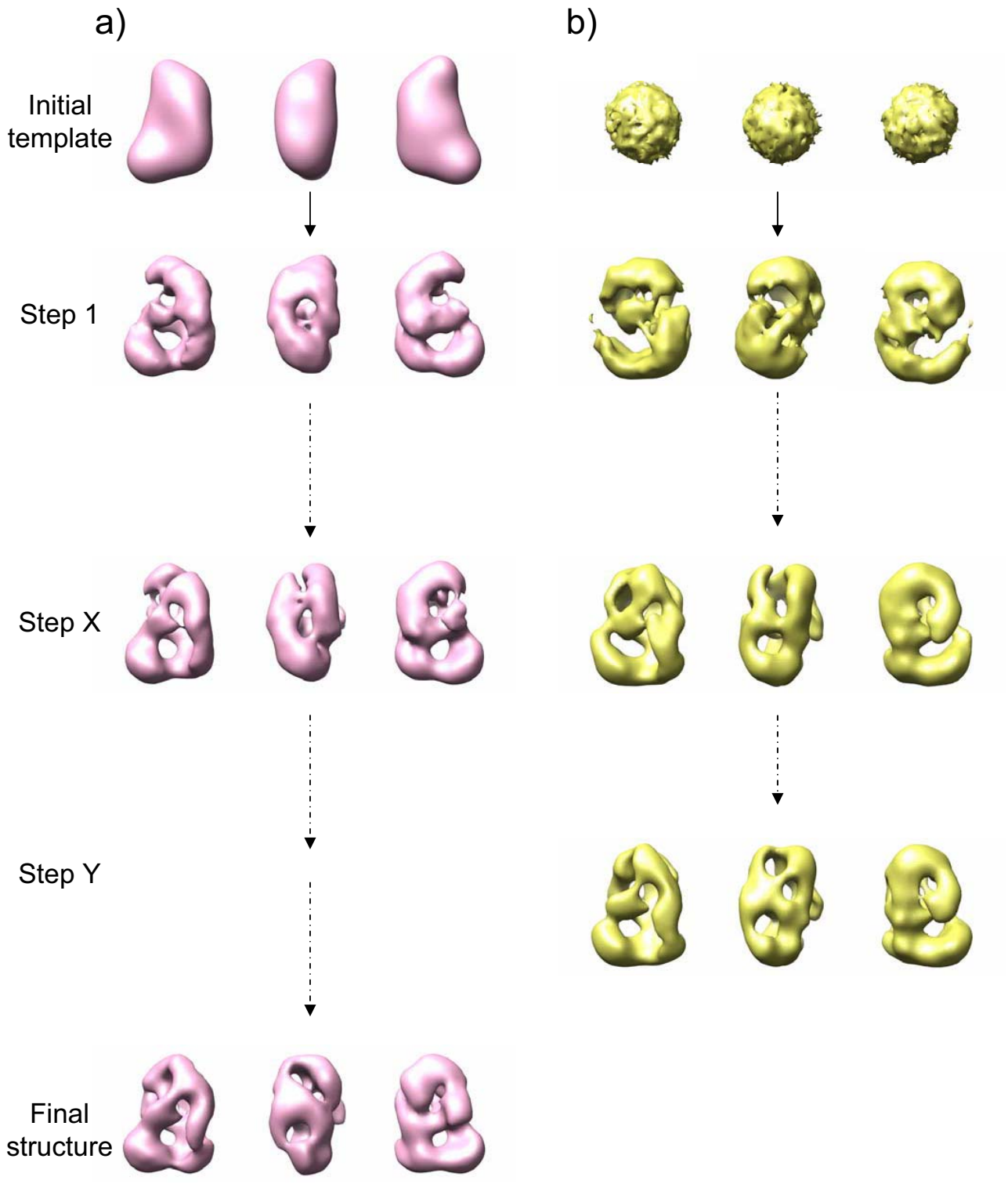
a)
b)
Initial template
Step 1
Step X
Step Y
Final structure
Refinement from C3b filtered to very low resolution
Refinement from noisy random Gaussian Blob

a)

Solution #	Correlation	Orientation (OK or flip)
1	0.780	flip
2	0.776	flip
3	**0.757**	**OK**
4	**0.757**	**OK**
5	0.755	flip
6	**0.755**	**OK**
7	**0.753**	**OK**
8	0.744	flip
9	0.743	flip
10	0.743	flip
11	**0.743**	**OK**
:	**:**	**:**
:	**:**	**:**
20	0.648	----
21	0.648	----

b)

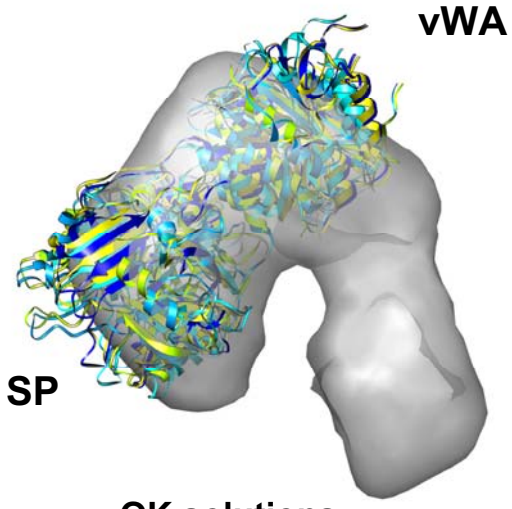

OK solutions

c)

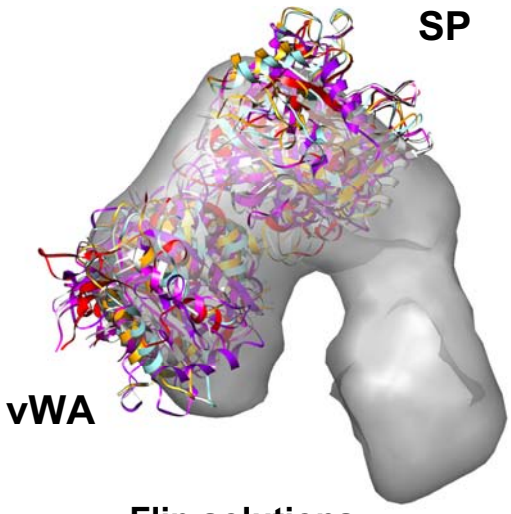

Flip solutions

d)

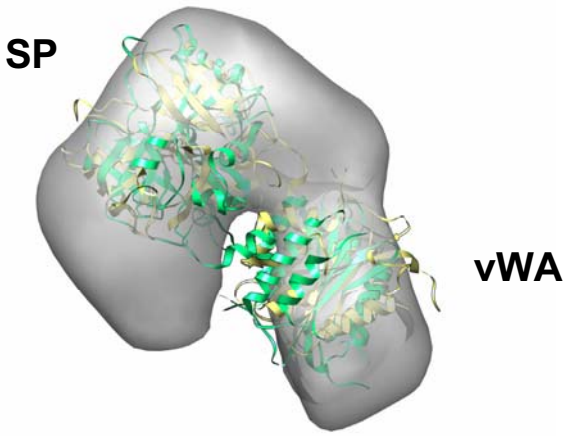

Low cross-correlation solutions

a)

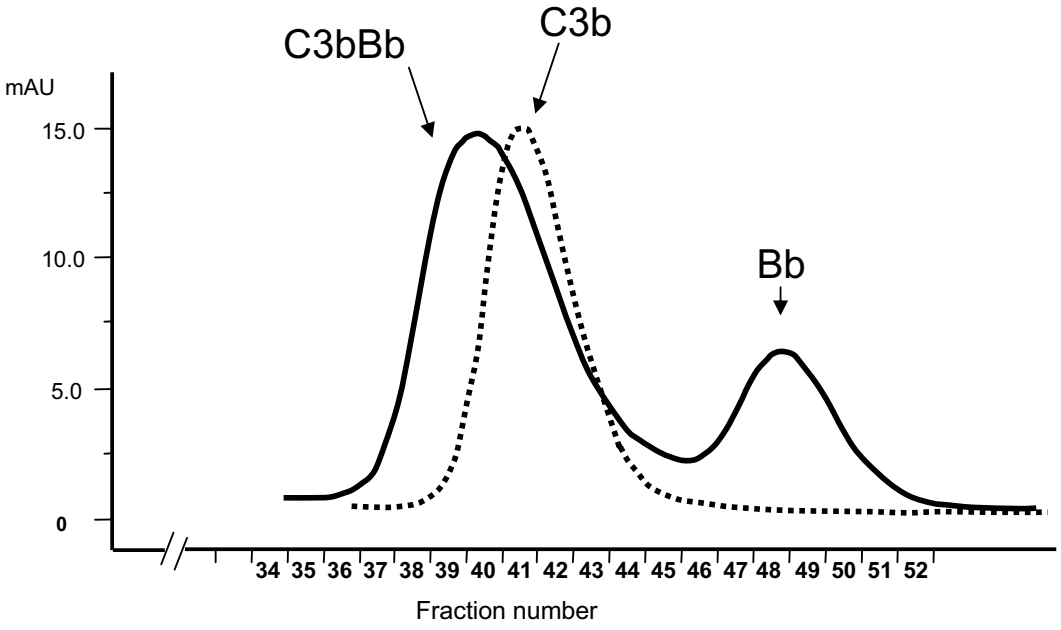
C3bBb
C3b
Bb
mAU
15.0
10.0
5.0
0
34 35 36 37 38 39 40 41 42 43 44 45 46 47 48 49 50 51 52
Fraction number

b)

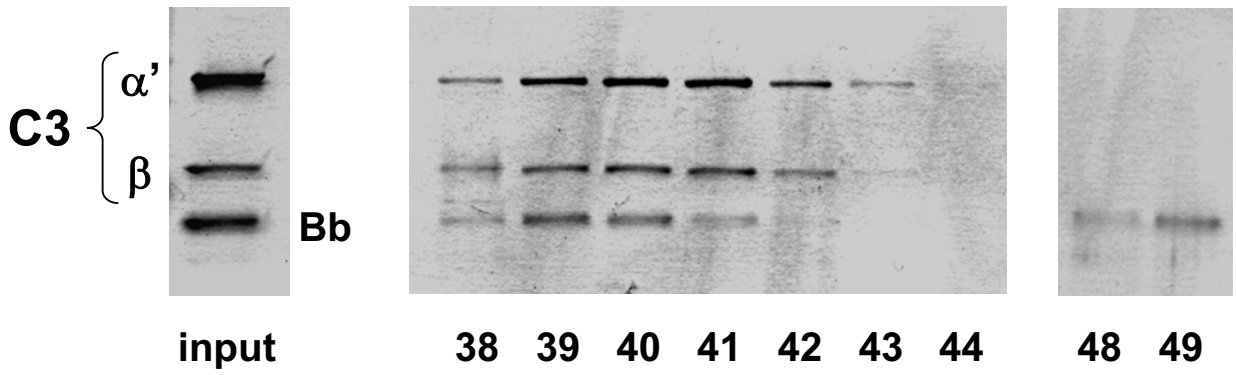
C3
α'
β
Bb
input
38 39 40 41 42 43 44
48 49